

Resonant activation of a Brownian particle out of a potential well: Microwave-enhanced escape from the zero-voltage state of a Josephson junction

Michel H. Devoret

*Department of Physics, University of California, Berkeley, California 94720,
Materials and Molecular Research Division, Lawrence Berkeley Laboratory, Berkeley, California 94720,
and Service de Physique du Solide et de Résonance Magnétique,
Centre d'Etudes Nucléaires de Saclay, 91191 Gif-sur-Yvette Cedex, France*

Daniel Esteve

*Service de Physique du Solide et de Résonance Magnétique,
Centre d'Etudes Nucléaires de Saclay, 91191 Gif-sur-Yvette Cedex, France*

John M. Martinis, Andrew Cleland, and John Clarke

*Department of Physics, University of California, Berkeley, California 94720
and Materials and Molecular Research Division, Lawrence Berkeley Laboratory, Berkeley, California 94720
(Received 31 December 1986)*

A current-biased Josephson tunnel junction in its zero-voltage state can be modeled as a Brownian particle in a potential well from which it can escape by thermal activation at a rate $\Gamma(0)$. The enhancement $\gamma = \Gamma(I_m)/\Gamma(0)$ of the escape rate has been measured in the presence of a microwave current of amplitude I_m , which represents a weak, sinusoidal force driving the particle. When the microwave frequency is varied, $\ln\gamma$ peaks approximately at the natural frequency at which the particle oscillates at the bottom of the anharmonic potential well. At higher frequencies, $\ln\gamma$ exhibits a sharp roll-off that steepens as the quality factor Q of the junction is increased, while at lower frequencies $\ln\gamma$ has a long tail with a shape which is almost independent of Q . These features are qualitatively consistent with the theories of Ivlev and Mel'nikov and Larkin and Ovchinnikov, which we discuss. These theories however, are not able to predict analytically the behavior of $\ln\gamma$ near the peak. To overcome this difficulty a detailed series of computer simulations has been performed. These simulations, together with certain scaling properties of the theories, have been used to construct an empirical formula for $\ln\gamma$ that is in qualitative agreement with the experimentally determined frequency dependence of $\ln\gamma$. The experimentally observed dependences of $\ln\gamma$ on temperature and microwave amplitude are in good quantitative agreement with predictions.

I. INTRODUCTION

This paper describes a phenomenon which we have observed in a current-biased Josephson tunnel junction^{1,2} and which we have called resonant activation.³ This effect combines two physical processes of long-standing importance:

- (i) The escape of a Brownian particle from a potential well, which is a model for the decay of metastable states in a wide variety of physical systems,⁴ and
- (ii) The pumping of energy into an anharmonic oscillator, a process which is central to a large range of non-linear effects.⁵

In thermal activation, a Brownian particle escapes from a potential well over a barrier [Fig. 1(a)] under the influence of a random fluctuating force [Fig. 1(b)]. The escape rate Γ is defined as the inverse of the average time that the particle, starting at the bottom of the well, takes to escape. In resonant activation the escape rate of the particle is enhanced by a weak oscillating force of amplitude A and frequency $\Omega/2\pi$ [Fig. 1(c)] superimposed on the random force. We define the enhancement as

$$\gamma(A, \Omega) = \Gamma(A, \Omega) / \Gamma(A = 0). \quad (1.1)$$

In this paper we confine our attention to the regime in which the oscillatory force makes only a weak perturbation on the dynamics of the Brownian particle. The opposite limit in which thermal fluctuations are small compared with the amplitude of the motion induced by the oscillatory force is an altogether different situation that has been widely studied, particularly in the case of the Josephson junction.^{6,7} For reasons that will become clear later, in the weak-perturbation regime it is useful to consider $\ln\gamma$ as the enhancement response, rather than the ratio γ .

In the weak-perturbation regime of present interest one naively expects that when $\Omega/2\pi$ is close to the natural frequency of oscillation in the well, energy will be transferred to the particle with a resulting *resonant* enhancement of the escape rate. As we shall see, generally speaking, this is what is observed both in experiments and in numerical simulations. However, the potential from which the particle escapes is anharmonic. This anharmonicity turns out to have a profound influence on

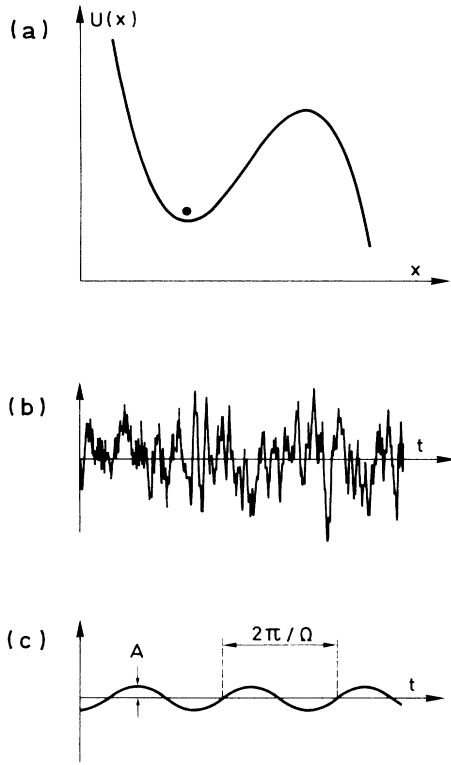


FIG. 1. (a) Potential well $U(x)$ from which a Brownian particle escapes over barrier; (b) random force to which particle is subjected; (c) oscillatory driving force superimposed on the random force to activate particle resonantly out of well.

the form of the resonant enhancement, which is quite different from the Lorentzian response of a simple classical harmonic oscillator subjected to an oscillating force. As we shall see, the resonance curve of the enhancement response has three striking features:

- (i) It is highly asymmetric, and exhibits a long tail on the low-frequency side,
- (ii) the maximum occurs at a frequency somewhat below the natural oscillation frequency, and
- (iii) the enhancement response drops steeply to zero as the frequency is increased above the natural frequency, the steepness becoming more pronounced as the damping is decreased.

As we shall see from our results and from theoretical investigations,⁸⁻¹⁰ these features arise from the variation of the oscillation frequency with the energy of the particle in the well; in contrast, the frequency of a simple harmonic oscillator is, of course, independent of energy, yielding a simple Lorentzian response curve. The understanding of the asymmetry of the enhancement is the main objective of this paper.

In our experiment, the position of the particle corresponds to the phase difference across a current-biased Josephson tunnel junction, while the oscillating force is provided by a small microwave current. This connection between the junction and Brownian motion is reviewed in Sec. II. In Sec. III we describe the experimental ap-

paratus, and in Sec. IV we present the results of a series of experiments. In Sec. V we discuss briefly several analytical models⁸⁻¹⁰ for resonant activation that were stimulated by our preliminary experiments.³ We also derive in this section a sum rule and the asymptotic behavior of the resonance for very high and very low frequencies. In Sec. VI we describe extensive numerical simulations that we have performed to study the dependence of the response on microwave frequency and amplitude as well as on the Q factor and temperature of the junction. To interpret our experimental results, in Sec. VI we also construct an empirical formula, with scaling provided by theory and a functional form verified by the numerical simulations. Section VII contains a concluding summary.

II. THE CURRENT-BIASED JOSEPHSON JUNCTION

We analyze the Josephson junction in terms of the resistively shunted junction model¹¹ shown in Fig. 2(a). The junction with critical current I_0 and self-capacitance C is shunted with a linear resistance R . The microwave source is represented by a current

$$I_m(t) = I_m \sin(\Omega t + \phi). \quad (2.1)$$

The Nyquist noise current $I_N(t)$ due to the resistor has a spectral density

$$S_{I_N}(\omega) = 2k_B T / \pi R \quad (2.2)$$

at angular frequency ω and temperature T ; k_B is Boltzmann's constant.

When biased with a constant current I , the junction can

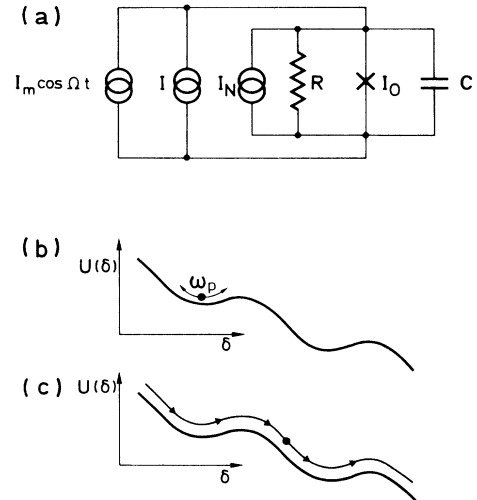


FIG. 2. (a) Model for Josephson junction with a constant current I and microwave current I_m . Tilted "washboard" potential model with (b) particle confined to a single potential well (corresponding to the zero-voltage state of the junction), and (c) particle running freely down the "washboard" (corresponding to the nonzero-voltage state of the junction).

be modeled as a particle moving in the one-dimensional tilted cosine potential¹² shown in Fig. 2(b),

$$U(\delta) = U_0(-s\delta - \cos\delta). \quad (2.3)$$

Here, $U_0 = I_0\Phi_0/2\pi$, $s = I/I_0$, $\Phi_0 = h/2e$, h is Planck's constant, and e is the electronic charge. The difference δ between the phases of the superconducting order parameters on the two sides of the junction corresponds to the position of the particle. The voltage V across the junction is related to the velocity of the particle by the Josephson relation¹

$$V = (\Phi_0/2\pi)\dot{\delta}. \quad (2.4)$$

By applying Kirchhoff's laws to the junction model and using Eq. (2.4), we obtain the following equation of motion:

$$C \left[\frac{\Phi_0}{2\pi} \right]^2 \ddot{\delta} + \left[\frac{\Phi_0}{2\pi} \right]^2 \frac{\dot{\delta}}{R} + \frac{\partial U(\delta)}{\partial \delta} = \frac{\Phi_0}{2\pi} [I_N(t) + I_m(t)]. \quad (2.5)$$

We see that C plays the role of the mass of the particle, while $1/R$ represents the damping. We emphasize at this point that both C and R may contain contributions from the bias circuitry.¹³ Equation (2.5) is a valid description of the junction provided the admittance of the bias circuitry can be represented as a capacitor in parallel with a resistor; in that case, C and R represent the combined capacitance and resistance of the junction and bias circuitry.

By applying a bias current I slightly less than I_0 one can prepare the particle in a local minimum of the tilted cosine potential [Fig. 2(b)]. In this metastable state, under the influence of the thermal and microwave currents, δ oscillates about a mean value in such a way that $\langle \dot{\delta} \rangle = 0$, and the junction is in the zero-voltage state. Eventually, the particle escapes from the well by passing over the top of the barrier; we assume that $k_B T \gg \hbar\omega_p$ so that macroscopic quantum tunneling¹⁴ of the particle through the barrier is completely negligible. We consider here only the case of a junction with a hysteretic I - V characteristic ($2\pi I_0 R^2 C \gg \Phi_0$) in which the damping is sufficiently low that the particle is never retrapped in another well after escaping from the initial metastable state. In this limit, after escaping the particle runs freely down the tilted cosine potential ($\langle \dot{\delta} \rangle > 0$) [Fig. 2(c)]. One monitors the escape by observing the onset of a voltage across the junction.

To facilitate comparison of theory and experiment we relate the parameters of the metastable, zero-voltage state shown in Fig. 1(a) to the electrical parameters appearing in Eq. (2.5). The barrier height is¹²

$$\Delta U = 2U_0[(1-s^2)^{1/2} - s \cos^{-1}s]. \quad (2.6)$$

which in the limit $s \rightarrow 1$ appropriate to the experiments can be approximated by¹¹

$$\Delta U = (4\sqrt{2}/3)U_0(1-s)^{3/2}. \quad (2.7)$$

The frequency $\omega_p/2\pi$ of small plasma oscillations at the bottom of the well is¹¹

$$\omega_p = \omega_{p_0}(1-s^2)^{1/4}, \quad (2.8)$$

where $\omega_{p_0} = (2\pi I_0/\Phi_0 C)^{1/2}$. The quality factor is

$$Q = \omega_p RC. \quad (2.9)$$

In the absence of a driving microwave current ($I_m = 0$), the escape of the particle occurs via thermal activation over the barrier at a rate⁴

$$\Gamma = a(\omega_p/2\pi)\exp(-\Delta U/k_B T). \quad (2.10)$$

The value of the prefactor a is close to unity. We shall adopt the theory of Büttiker *et al.*¹⁵ that yields, for $Q \gtrsim 5$,

$$a_{\text{BHL}} = 4\alpha / [(1 + \alpha Q k_B T / 1.8 \Delta U)^{1/2} + 1]^2, \quad (2.11)$$

where α is of the order of unity. These authors found a best fit to numerical simulations with $\alpha = 1$, although Risken and Voigtlaender¹⁶ have proposed that the correct value of α is 1.4738... In this paper we require a knowledge of the prefactor only to check our numerical simulations in the absence of a driving force; we believe the value of γ is insensitive to small changes in the prefactor.

Thus, in the absence of an oscillating driving term, the escape rate from the zero voltage state is a function of the parameters ΔU , ω_p , Q , and T . We turn now to an experimental investigation of the effects of an oscillatory current, which introduces two additional parameters, namely I_m and $\Omega/2\pi$.

III. EXPERIMENTAL APPARATUS

The purpose of the experiment is to measure the escape rate of a Josephson tunnel junction from the zero-voltage state as a function of bias current and microwave frequency at several values of temperature and microwave power. The experimental apparatus is shown schematically in Fig. 3. A very important feature is the extensive radio-frequency (rf) and microwave low-pass filtering used to isolate the junction from room-temperature thermal noise and external spurious parasitic noise sources. The rf filters, which consisted of a simple RC network with a 3-dB point of about 1 MHz, provided more than 60 dB of attenuation from 20 to 200 MHz. However, at higher frequencies the attenuation was appreciably smaller, presumably because of stray impedances across the filter elements. Consequently, we developed a novel type of microwave filter, consisting of a spiral coil of insulated manganin wire inside a copper tube filled with 30- μm -diam copper powder. Since each grain is apparently insulated from its neighbors by a naturally grown oxide layer, the effective surface area is enormous, and the skin-effect losses are substantial. The measured attenuation of a filter 0.1 m long was greater than 50 dB from 0.5 to 12 GHz at room temperature. Two of these filters in series were immersed in the helium bath.

The junction was mounted at the end of a third microwave low-pass filter (similar to the other two) shown schematically in Fig. 4. The attenuation of this mount was about 10 dB. The mount was designed to minimize standing electromagnetic waves in the leads connected to the junction. It is important to emphasize that at the

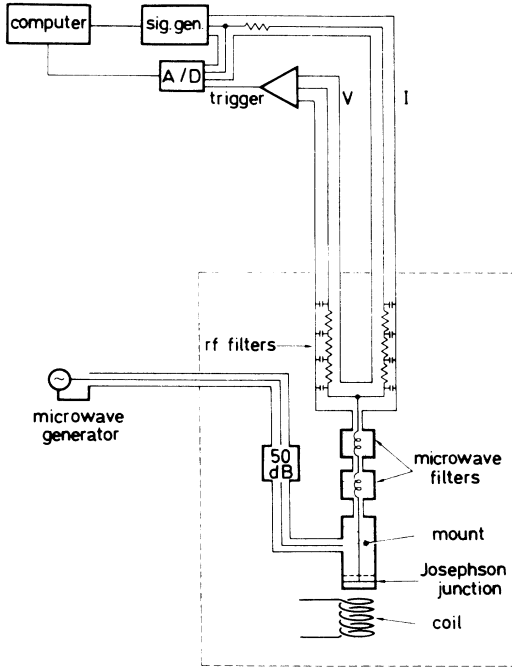


FIG. 3. Configuration of experiment to measure the rate of escape of a current-biased Josephson junction from the zero-voltage state in the absence and presence of a microwave-driving force. Components in dashed box are immersed in liquid helium.

plasma frequency the dissipation in the mount completely dominated the intrinsic quasiparticle damping of the junction. On the other hand, the reactance presented by the mount to the junction was a relatively small perturbation on the junction self-capacitance. A connector at the midpoint of the mount was used to couple microwave power capacitively to the central conductor. The high impedance of this coupling ensured that the junction was irradiated with a current source.

The Nb-NbO_x-PbIn tunnel junctions were fabricated on (10×10)-mm² oxidized silicon chips in a cross-strip geometry with a nominal area of 100 μm². The junction was connected to the mount with indium pads in a two-terminal arrangement. A magnetic field could be applied in the plane of the junction by means of a solenoid in order to adjust the critical current. The *I*-*V* characteristics

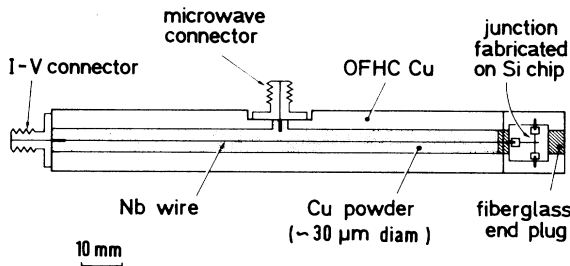


FIG. 4. Attenuating mount to which junction is attached.

of the junctions exhibited very low leakage at voltages below the sum of the energy gaps. The mount and the various filters were immersed in liquid helium, which could be pumped down to 1.2 K.

IV. EXPERIMENTAL PROCEDURES AND RESULTS

A. Determination of I_0

To determine the parameter $s = I/I_0$ one needs to measure I_0 as accurately as possible. We measure I_0 by determining the lifetime of the zero-voltage state in the absence of microwaves. In this method one applies a current I increasing linearly in time to the junction, and determines the value of current ($< I_0$) at which a voltage appears. One repeats the procedure a large number of times (10^4 – 10^5 in our experiments) to acquire a distribution of currents $P(I)$ at which the junction escapes from the zero-voltage state. The escape rate is found from¹²

$$\Gamma(I) = \frac{1}{\Delta I} \frac{dI}{dt} \ln \left[\frac{\sum_{i \geq I} P(i)}{\sum_{i \geq I + \Delta I} P(i)} \right]. \quad (4.1)$$

Here, dI/dt is the current ramp rate and ΔI is the channel width in the analog-to-digital converter used to record I . Typically, we measured escape rates in the range 10^2 – 10^5 s⁻¹.

Having determined $\Gamma(I)$, we find I_0 by plotting $\{\ln[\omega_p(I)/2\pi\Gamma(I)]\}^{2/3}$ vs I . For the purpose of determining I_0 it is sufficient here to take $a = 1$. In the limit in which the cubic approximation is valid, we see from Eqs. (2.7) and (2.10) that the data should lie on a straight line with slope $(I_0\Phi_0 2\sqrt{2}/3\pi k_B T)^{2/3}$ intersecting the current axis at I_0 . Examples of our data are shown in Fig. 5 for four different temperatures. Each set of data lies along a straight line with a slope that yields a temperature in very good agreement with the measured bath temperature. The good agreement of the bath temperature and the effective temperature measured by thermal activation together with the lack of any observable curvature in the data constitute an important check that external noise is negligible.

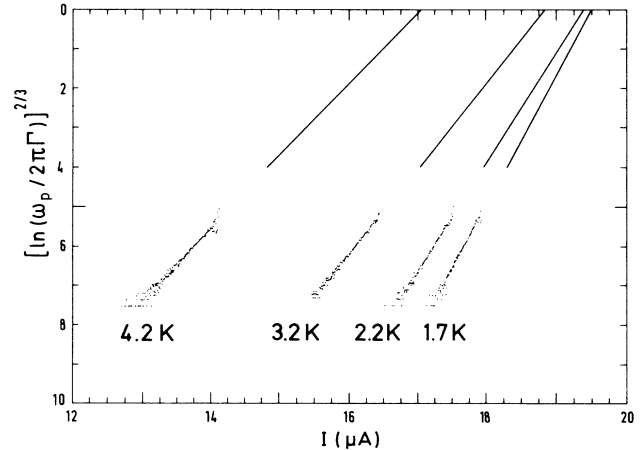


FIG. 5. Plots of $\{\ln[\omega_p/2\pi\Gamma]\}^{2/3}$ vs bias current I at four temperatures in the absence of microwave power.

B. Determination of resonant activation response curve

Although the current ramp method provides a straightforward means of measuring $\Gamma(I)$, it explores only a limited region of the resonance. To determine *changes* in Γ due to the microwaves with greater accuracy and over a greater range of microwave frequency, we measured the lifetime directly at a fixed value of bias current while sweeping the microwave frequency through the plasma resonance. In this method, we applied a 10-kHz square wave current, and measured the average time that elapsed between the leading edge of the square wave and the junction-switching pulse. The precision obtainable with this technique was around 1% in 1 s. Figure 6 shows an example of the time distribution of 10^4 switching events for a fixed current; this distribution is exponential and its slope provides a measurement of Γ in good agreement with that measured by the first method.

The measurement of Γ in the presence of microwaves is complicated by the fact that the microwave-current amplitude I_m injected into the junction varies as the frequency is swept. To circumvent this problem, we use a technique somewhat analogous to lock-in detection, in which we measure the enhancement ratio at two slightly different values of ω_p while $\Gamma(0)$ remains fixed. This we accomplish by adjusting I_0 (by means of a magnetic field) and I simultaneously so that $\Gamma(0)$ remains fixed (an example of data obtained in this way is shown in Fig. 7). We operate with small enough microwave power for the enhancement to be proportional to I_m^2 (see below and next section) so that we can write

$$\ln \gamma = I_m^2(\Omega) g(\Omega, \omega_p). \quad (4.2)$$

The change in the enhancement when the plasma frequency is changed by $\Delta\omega_p$, written as

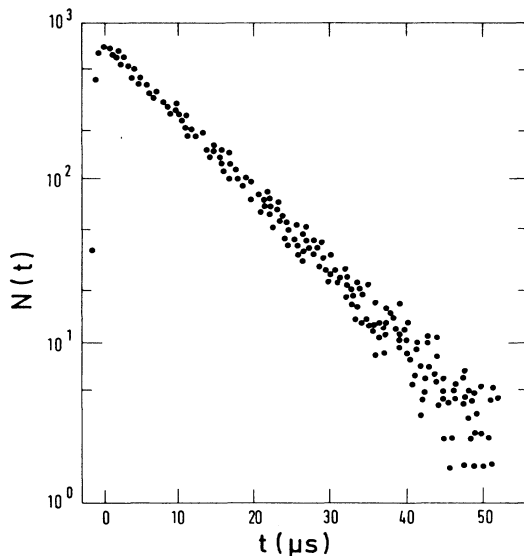


FIG. 6. Distribution of switching events in absence of microwaves for junction *A* at 4.2 K with parameters listed in Table I.

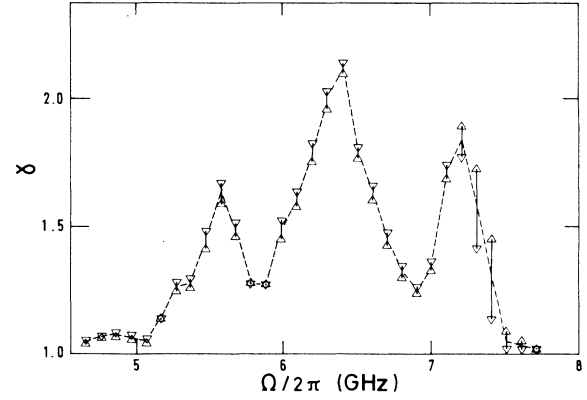


FIG. 7. Measured values of the enhancement ratio γ vs microwave frequency at 4.2 K for two different values of I_0 with the same $\Gamma(0) = 0.12 \times 10^6 \text{ s}^{-1}$. Upward-pointing triangles, $I_0 = 6.22 \text{ } \mu\text{A}$, $I = 4.39 \text{ } \mu\text{A}$; downward-pointing triangles, $I_0 = 5.92 \text{ } \mu\text{A}$, $I = 4.19 \text{ } \mu\text{A}$. Dashed line is drawn through the mean value of γ at each frequency. Other junction parameters are listed in Table I (junction *A*).

$$\Delta \ln(\ln \gamma) = \Delta \omega_p \frac{\partial \ln g}{\partial \omega_p}, \quad (4.3)$$

is independent of $I_m(\Omega)$. Assuming $g(\Omega, \omega_p) = g(\Omega - \omega_p)$ we can rewrite Eq. (4.3) as

$$\Delta \ln(\ln \gamma) = -\Delta \omega_p \frac{\partial \ln g}{\partial \Omega}. \quad (4.4)$$

The two experimental enhancement curves intersect at a frequency $\Omega_{\text{max}}/2\pi$ at which the slope of the reduced response $g(\Omega)$ is zero. One obtains a reconstructed $\ln \gamma$ (denoted $\ln \gamma^{\text{rec}}$) by integrating separately from Ω_{max} in the direction of increasing and decreasing frequency:

$$\ln \gamma^{\text{rec}}(\Omega) = \exp \left[-\frac{1}{\Delta \omega_p} \int_{\Omega_{\text{max}}}^{\Omega} \Delta \ln(\ln \gamma) d\Omega' \right]. \quad (4.5)$$

The relation between $g(\Omega)$ and $\ln \gamma^{\text{rec}}$ is $g(\Omega) = g(\Omega_{\text{max}}) \ln \gamma^{\text{rec}}$; $g(\Omega_{\text{max}})$ cannot be found by this method but is only a scale factor. We have tested this technique on artificially generated data and found that it reconstructs the enhancement with sufficient accuracy. For our experimental results, we quote the average values of I and I_0 .

The result of applying this technique to the raw data of Fig. 7 is shown in Fig. 8(a), where we plot $\ln \gamma^{\text{rec}}$ versus frequency. In contrast to the raw data, the reconstructed enhancement is a smooth function of the microwave frequency.

C. Experimental results

We have investigated the dependence of $\ln \gamma$ on three parameters: the frequency and amplitude of the microwave current and the temperature.

Figures 8 and 9 show the enhancement $\ln \gamma^{\text{rec}}$ obtained at 4.2 K for three junctions; the relevant parameters are listed in Table I. In Figs. 8 and 9(a) the junctions were

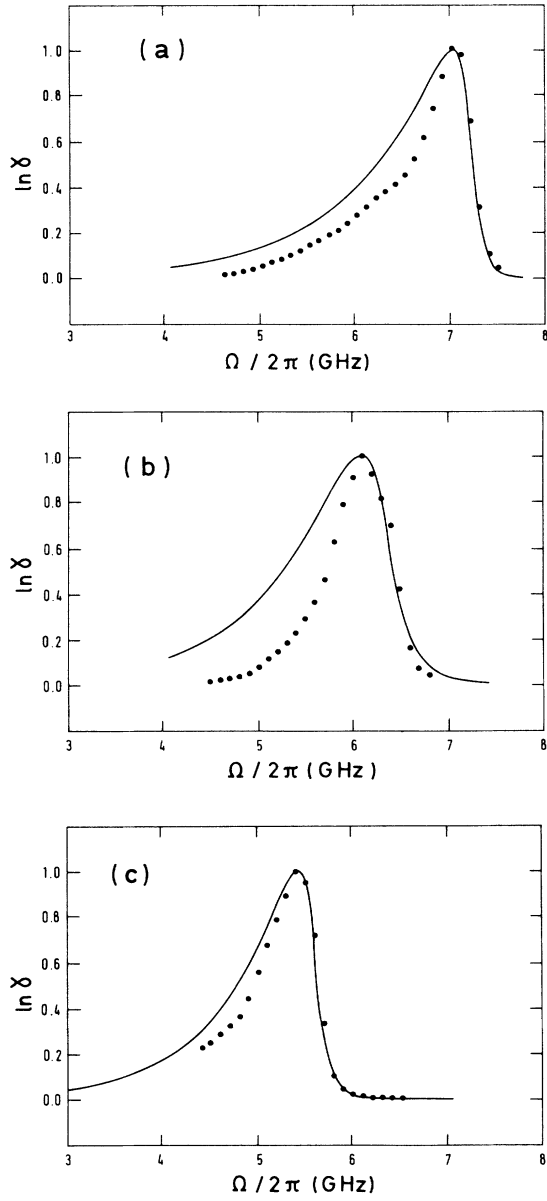


FIG. 8. Resonant activation curves, $\ln \gamma$ vs $\Omega/2\pi$, at 4.2 K for junction *A* (unshunted junction) at three values of the critical current. (a) $I_0 = 6.07 \mu\text{A}$; (b) $I_0 = 4.64 \mu\text{A}$; (c) $I_0 = 3.42 \mu\text{A}$. Dots are experimental data; curves are fits of Eqs. (6.4) and (6.5) to the data.

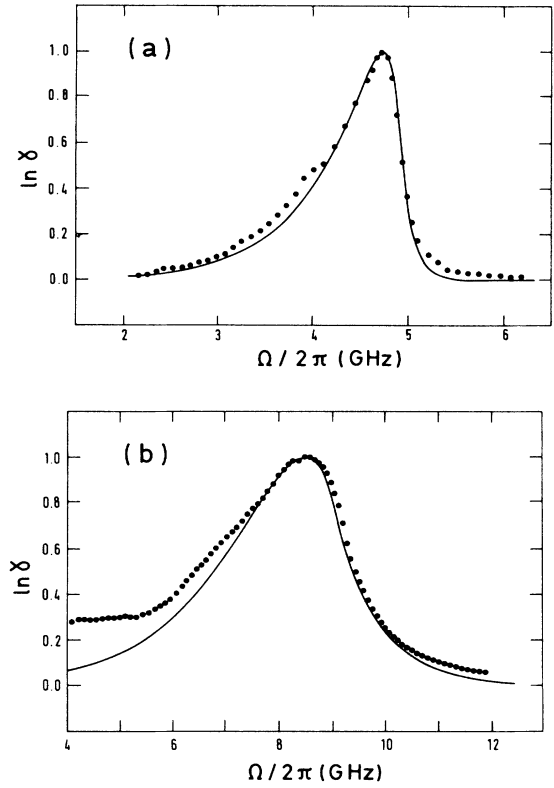


FIG. 9. Resonant activation curves, $\ln \gamma$ vs $\Omega/2\pi$, at 4.2 K for two different junctions. (a) Junction *B* (unshunted); (b) junction *C* (shunted with a 10.7- Ω thin-film resistor). Dots are experimental; curves are fits of Eqs. (6.1) and (6.5) to the data.

unshunted, while in Fig. 9(b) a normal-metal shunt was evaporated on the substrate before the niobium and lead films were deposited. The three sets of data in Fig. 8 were taken at different values of the critical current obtained by the application of a magnetic field to the junction. The experimental data in Fig. 8(b) are those published previously.³ Each curve is clearly asymmetric about its maximum, rolling off much more rapidly on the high-frequency side than on the low-frequency side. The maximum for the shunted junction in Fig. 9(b) is much broader than the maxima for the unshunted junctions, as

TABLE I. Parameters of three junctions *A*, *B*, and *C* for which resonant activation curves are plotted in Figs. 8 and 9. The values of $\omega_p^{\text{fit}}/2\pi$ and λ^{fit} are obtained from the best fits of Eq. (6.5) to the data. The estimate of Q is from the dashed line in Fig. 19, while C and R are deduced from Eqs. (2.8) and (2.9).

Junction	Fig.	I_0 (μA)	I (μA)	R_{shunt} (Ω)	$\omega_p^{\text{fit}}/2\pi$ (GHz)	λ^{fit}	Q	C (pF)	R (Ω)
<i>A</i>	8(a)	6.07	4.26	no shunt	7.4 ± 0.1	70 ± 14	35 ± 7	6.3 ± 0.1	120 ± 25
<i>A</i>	8(b)	4.64	3.07	no shunt	6.5 ± 0.1	30 ± 5	15 ± 2	6.6 ± 0.1	55 ± 11
<i>A</i>	8(c)	3.42	1.94	no shunt	5.7 ± 0.1	50 ± 10	25 ± 2	6.8 ± 0.1	95 ± 10
<i>B</i>	9(a)	3.09	1.62	no shunt	5.0 ± 0.1	40 ± 8	20 ± 4	8.4 ± 0.1	75 ± 8
<i>C</i>	9(b)	22.96	19.93	10.7	9.0 ± 0.1	11 ± 2	5 ± 1	10.9 ± 0.1	8 ± 2

we expect for a junction with a lower Q .

In Fig. 10 we plot $\ln\gamma$ vs I_m^2 for junction C at three microwave frequencies. The central frequency corresponds to the maximum in Fig. 9, while the other two frequencies are above and below the maximum. It should be emphasized that, because of the frequency-dependent microwave coupling, the arbitrary scale in I_m^2 is different for each frequency. At all three frequencies we observe that $\ln\gamma$ scales linearly with I_m^2 , that is, with the microwave power, for $\ln\gamma \lesssim 1$; at higher values of $\ln\gamma$, the enhancement rolls off. This linear dependence is the motivation for our focusing on $\ln\gamma$ rather than γ .

In Fig. 11 we show $\ln\gamma$ vs I_m^2 for junction C at fixed microwave frequency at four values of temperature and under the following conditions that keep $\Delta U/k_B T$ constant: We choose values of I_0 and I so that both $\Gamma(0)$ and ω_p have the same values at all temperatures; the microwave frequency is set equal to $\omega_p/2\pi$. Since the microwave-power and frequency settings are kept fixed, the I_m^2 axis is the same for all four temperatures. We observe that $\ln\gamma$ increases as the temperature is lowered; in fact, $(\ln\gamma)/I_m^2$ scales as $1/T$, as indicated in the inset.

This concludes our presentation of the experimental data. To interpret them, we now turn to a discussion of the theory of resonant activation.

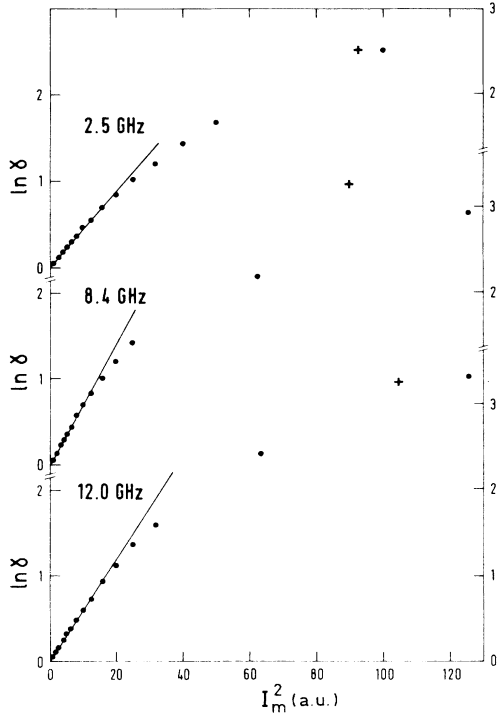


FIG. 10. $\ln\gamma$ vs I_m^2 for junction C at 4.2 K and at three microwave frequencies (solid circles). At each frequency a single point (+) has been plotted corresponding to the simulations shown in Fig. 15.

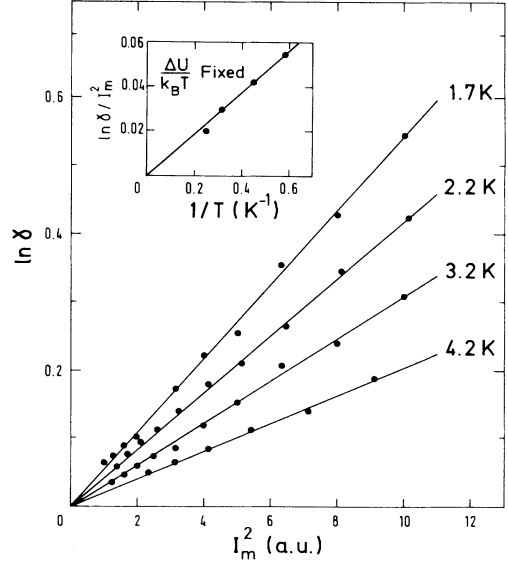


FIG. 11. $\ln\gamma$ vs I_m^2 for junction C at four temperatures. The data were taken with $\Delta U/k_B T = \text{const}$ and $\Omega = \omega_p$ (see text). Inset shows $(\ln\gamma)/I_m^2$ vs $1/T$ at fixed $\Delta U/k_B T$.

V. THEORIES OF RESONANT ACTIVATION

To facilitate further discussion, it is convenient first to cast the dynamical equations of Sec. II into dimensionless form.

A. Dimensionless equations

In the limit $s \rightarrow 1$ which is relevant to the experimental situation, the potential $U(\delta)$ is cubic and the equation of motion, Eq. (2.5), can be written in the dimensionless form

$$\frac{\partial^2 x}{\partial \tau^2} + \frac{1}{Q} \frac{\partial x}{\partial \tau} + \frac{\partial}{\partial x} \left[\frac{x^2}{2} - \frac{1}{3\sqrt{6}} x^3 \right] = \zeta(\tau) + A \sin(F\tau + \phi). \quad (5.1)$$

We have introduced the reduced position x and time τ given by

$$x = (4/\sqrt{6})(1-s)^{1/2}(\delta - \delta_0) \quad (5.2)$$

and

$$\tau = \omega_p t, \quad (5.3)$$

where the phase difference $\delta_0 = \sin^{-1}s$ is the position of the local potential minimum. In Eq. (5.1), the barrier height is unity, the period of oscillation at the bottom of the well is 2π , and the spectral density of the current noise $\zeta(\tau)$ is fixed by

$$\langle \zeta(0)\zeta(\tau) \rangle = (2\Theta/Q)\delta(\tau), \quad (5.4)$$

where $\delta(\tau)$ is the Dirac δ function. The parameters Θ , A , and F are the reduced temperature, and reduced ampli-

tude and frequency of the driving force:

$$\Theta = k_B T / \Delta U, \quad (5.5)$$

$$A = I_m / (\Delta U C \omega_p^2)^{1/2}, \quad (5.6)$$

and

$$F = \Omega / \omega_p. \quad (5.7)$$

To our knowledge, there is no direct analytical solution of the stochastic equation of motion, Eq. (5.1), for the enhancement of the escape rate by the oscillating driving term. Rather, one makes the basic assumption that γ is proportional to the enhancement in the thermal equilibrium probability of finding the particle at the top of the barrier. Thus, one neglects any depletion of the population by the escape process. Under this assumption, one is required to solve the time-dependent Fokker-Planck equation associated with the Langevin equation (5.1). Unfortunately, even this task cannot be carried out exactly because of the anharmonicity of the potential.

It is worth emphasizing that the anharmonic term in Eq. (5.1) is fundamental to the shape of the resonant enhancement response curve, and cannot be treated merely as a perturbation on a quadratic potential. To stress this point, before embarking on detailed calculations of resonant activation we give a brief qualitative discussion. Consider first a quadratic potential truncated at x_b to give the same barrier height as that in the quadratic plus cubic potential [Fig. 12(a)]. The frequency of oscillation is constant for all energies E up to ΔU , as shown in Fig. 12(b), where we have given a width $\Delta\omega = 1/RC$ to the oscillation frequency arising from the finite Q . If one now applies an oscillating force to the system, we expect the particle to

absorb energy resonantly at $\omega = \omega_p$. Thus the enhancement will be a Lorentzian centered at ω_p , as indicated in Fig. 12(c). On the other hand, if we consider the quadratic plus cubic potential shown in Fig. 12(d), the frequency is no longer independent of the energy E of the particle, but decreases smoothly to zero as the energy approaches ΔU ; again we have given a width to the oscillation frequency to represent a finite Q . Because of the distribution of oscillation frequencies due to $\omega(E)$, the enhancement in the presence of microwaves is now expected to have a broad and highly asymmetric frequency dependence. The rounding introduced by the finite Q pulls the peak away from ω_p towards low frequencies. There is now a long tail on the low-frequency side, corresponding to the fact that the oscillation of the particle near the top of the well occurs at frequencies below ω_p . The high-frequency side, on the other hand, cuts off more sharply than the low-frequency side because the particle no longer responds to frequencies greater than ω_p as soon as it is excited to energies above the bottom of the well.

We now turn to a quantitative discussion of these effects, returning first to the truncated harmonic potential model which, although it cannot account for the asymmetry in the data, nonetheless yields certain scaling properties that are correct.

B. The truncated harmonic potential

The potential for this model³ is shown in Fig. 12(a). The smooth nonlinearity of the cubic potential is replaced with a sharp discontinuity at a single point. In the absence of the oscillatory driving term the escape rate is proportional to the probability (in the untruncated potential) that $x = x_b$:

$$P(x = x_b) = (1/N) \exp(-x_b^2 / 2\Theta). \quad (5.8)$$

Here, $P(x)$ is the probability for the particle to be in the interval $[x, x + dx]$, and $1/N$ is a normalization factor independent of A and F . In the presence of the microwave-driving term and in the absence of noise, the displacement $x_m(\tau)$ is given by

$$x_m(\tau) = \text{Re} \left[\frac{A \exp[i(F\tau + \phi)]}{(1 - F^2) + iF/Q} \right]. \quad (5.9)$$

The mean-square value is

$$\langle x_m^2 \rangle_\phi = A^2 / 2[(1 - F^2)^2 + F^2/Q^2], \quad (5.10)$$

where $\langle \dots \rangle_\phi$ denotes an average over the phase ϕ .

Since the equation of motion is linear, its solution when both the microwave and noise terms are present is

$$x(\tau) = x_N(\tau) + x_m(\tau), \quad (5.11)$$

where x_N is the solution of the presence of the noise current only and x_m is the solution in the presence of the microwave current only. The probability that $x = x_b$ now takes the form

$$P(x = x_b) = P(x_N = x_b - x_m) \quad (5.12)$$

or

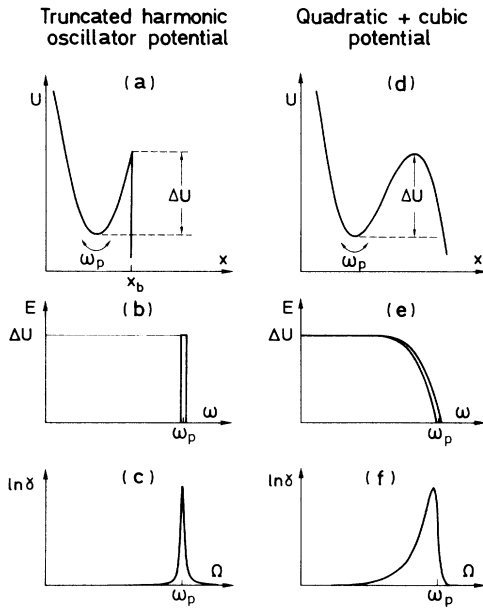


FIG. 12. Sketches of U vs x , E vs ω , and $\ln \gamma$ vs Ω for (a) the truncated harmonic-oscillator potential and (d) quadratic plus cubic potential; (b), (c), (e), and (f) are plotted for $Q = 30$.

$$P(x=x_b) = \langle (1/N) \exp[-(x_b - x_m)^2 / 2\Theta] \rangle_\phi. \quad (5.13)$$

We assume that the microwave perturbation is very small, so that x_m is also correspondingly small. Expanding the exponential in Eq. (5.13) and noting that $\langle x_m \rangle_\phi = 0$, we find, to second order in x_m ,

$$P(x=x_b) = \frac{1}{N} \exp(-x_b^2 / 2\Theta) \left[1 + \frac{1}{\Theta} \left(\frac{x_b^2}{2\Theta} - \frac{1}{2} \right) \langle x_m^2 \rangle_\phi \right]. \quad (5.14)$$

Combining Eqs. (5.8), (5.10), and (5.14), we find, to second order in A ,

$$\ln \gamma = \ln \left[\frac{P(x_b, A)}{P(x_b, 0)} \right] = \frac{1}{2\Theta} \left[\frac{1}{\Theta} - \frac{1}{2} \right] \frac{A^2}{(1-F^2)^2 + F^2/Q^2}. \quad (5.15)$$

As expected, in the weak-perturbation limit this model predicts a Lorentzian resonance centered at the natural frequency of oscillation. The width of the resonance scales with Q , and for $\Theta \ll 1$ the height is proportional to $Q^2 A^2 / \Theta^2$. As we shall see presently, the model does give the correct dependence on A and, for $\Theta \ll 1$, on Θ , but *the shape of the resonance and the dependence on Q are incorrect.*

The failure of the linear equation to produce the observed shape of the resonance shows the important role played by the anharmonicity in the phenomenon and forces one to solve the much more difficult problem in which the cubic term is retained in Eq. (5.1).

C. Sum rule

Before describing the theories of resonant activation, we derive here a general result that imposes a constraint on the overall magnitude of the enhancement of the escape rate in the presence of microwaves.

We have shown that in the limit of small microwave power there is a linear relationship between the enhancement and the square of the applied oscillating microwave current. We write

$$\ln \gamma = A^2 f(\Theta, F, Q) \quad (5.16)$$

or, using the definition of A ,

$$\ln \gamma = (RI_m^2 / \Delta U Q \omega_p) f(\Theta, F, Q). \quad (5.17)$$

This result simply reflects the fact that the energy communicated to the particle in the well by the microwave current is proportional to the microwave power.

We now propose that this linear relationship between the microwave power and $\ln \gamma$ remains valid in the case where the irradiation consists of broadband Gaussian noise with spectral density $S_N(\Omega)$. We then write

$$\ln \gamma_N = \frac{2R}{\Delta U Q \omega_p} \int d\Omega f(\Theta, \Omega / \omega_p, Q) S_N(\Omega). \quad (5.18)$$

The factor of 2 arises from the fact that the spectral density of $I_m \sin \Omega_0 t$ is

$$S(\Omega) = I_m^2 \delta(\Omega - \Omega_0) / 2. \quad (5.19)$$

We now investigate the consequences of the hypothesis, Eq. (5.18), when $S_N(\Omega)$ is frequency independent (white noise). In that case, the irradiation is indistinguishable from an added thermal noise corresponding to a temperature increase T_N of the resistor R . Using the Nyquist formula we find

$$S_N(\Omega) = \frac{2}{\pi} \frac{k_B T_N}{R}, \quad (5.20)$$

which, with Eq. (5.18), yields

$$\ln \gamma_N = \frac{4}{\pi} \frac{k_B T_N}{\Delta U Q} \int_0^\infty dF f(\Theta, F, Q). \quad (5.21)$$

On the other hand, we can compute γ_N directly using Kramer's equation (2.10) for a resistor at temperature $T + T_N$:

$$\ln \gamma_N = - \frac{\Delta U}{k_B(T + T_N)} + \frac{\Delta U}{k_B T}. \quad (5.22)$$

In Eq. (5.22) we have neglected higher-order terms in $\Delta U / k_B T$ arising from the prefactor in the expression of Γ .

Combining Eqs. (5.21) and (5.22) and using $\Theta = k_B T / \Delta U$, we finally arrive at

$$\int_0^\infty dF f(\Theta, F, Q) = \frac{\pi Q}{4\Theta^2} + O\left(\frac{1}{\Theta}\right). \quad (5.23)$$

In terms of more directly accessible quantities, this last equation becomes

$$\int_0^\infty d\Omega \ln \gamma(\Delta U, T, \Omega, \omega_p, Q) = \frac{\pi}{4} \frac{RI_m^2}{k_B T} \frac{\Delta U}{k_B T} + O\left(\frac{\Delta U}{k_B T}\right). \quad (5.24)$$

We see that the area under the resonance curve scales simply as $\Delta U / (k_B T)^2$ and should be linear in the resistance. It is interesting to note that these scaling properties, which were already displayed in the particular case of the truncated harmonic-oscillator model, are general and do not depend on the exact shape of the potential.

D. Theories of resonant activation in an anharmonic potential

Grigolini and Fonseca⁸ were the first to develop a theory for our experimental results.³ In their theory the main effect of the oscillating force is to increase the diffusion coefficient of the particle when the energy-dependent oscillation frequency coincides with the frequency of the driving force. This theory leads to a set of differential equations that are solved numerically, but unfortunately do not show a pronounced asymmetry in the resonance curve. Two other theories, each starting from a very different viewpoint but reaching similar conclusions, were subsequently put forward. Ivlev and Mel'nikov⁹ (IM), starting with the classical equation of motion, obtain a simplified Fokker-Planck equation for the energy that precisely keeps track of the energy imparted to the particle by the oscillating force. These authors solve the equation analytically in various limiting cases. Larkin and

Ovchinnikov¹⁰ (LO) write an equation for the evolution of a quantum density matrix, limited to diagonal and next-to-diagonal terms, using the eigenstates of the unperturbed system as a basis set. The matrix elements of the operator \hat{x} between two adjacent energy levels separated by an energy Δ are calculated using a semiclassical approximation. The theory leads to a pair of coupled differential equations that are solved numerically, yielding an asymmetric response curve in qualitative agreement with experimental data. Furthermore, in the limit of high Q , LO provide analytical predictions that agree with those of IM. Since these results give considerable insight into the physics of the problem, we summarize them at this point.

When $\frac{36}{5} \ll Q \ll 36/5\Theta$ and $A \ll 1$, IM and LO predict¹⁷ that, for $F < 1$,

$$\ln \gamma_{<} = \frac{\pi Q A^2 \omega_p}{4\Theta^2 \Delta U} \left. \frac{d\omega(E)}{dE} \right|_F^{-1}, \quad (5.25)$$

where $\omega(E)$ is the oscillation frequency in the cubic potential at energy E . The subscript F implies that the derivative is evaluated where $\omega/2\pi$ is equal to the microwave frequency. We have computed $d\omega(E)/dE$ numerically and plotted it in Fig. 13. At $F=1$, Eq. (5.25) takes the value

$$\ln \gamma_{<}(F=1) = 9\pi Q / A^2 5\Theta^2. \quad (5.26)$$

For driving frequencies above the plasma frequency ($F > 1$), IM and LO find

$$\ln \gamma_{>} = \frac{9\pi Q A^2}{5\Theta^2} \frac{1}{1 + \exp[2\pi Q(F-1)]}, \quad (5.27)$$

which, at $F=1$, takes the value

$$\ln \gamma_{>}(F=1) = 9\pi Q A^2 / 10\Theta^2. \quad (5.28)$$

Equations (5.26) and (5.28) do not match in the vicinity of $F=1$. However, Eqs. (5.25) and (5.27) make several predictions that are extremely useful above and below the resonance:

- (i) $\ln \gamma$ is proportional to A^2/Θ^2 as for the truncated

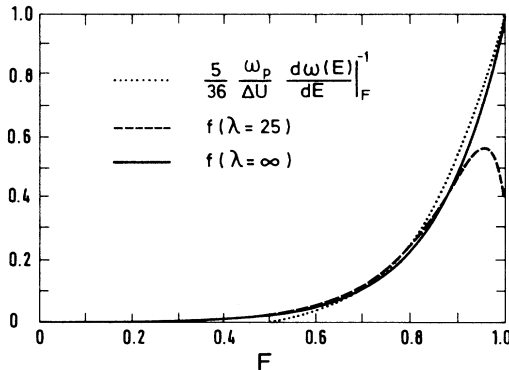


FIG. 13. Numerical calculation of $[7.2 d\omega(E)/dE |_F]^{-1}$ for "washboard" potential vs F (dotted line). Also shown is $f(F)$ for $\lambda = \infty, 25$ [Eq. (6.2)].

harmonic potential and in agreement with the sum rule of Eq. (5.24); in fact, $\int_0^{\omega_p} d\Omega \ln \gamma_{<}$ obeys the sum rule exactly.

(ii) For $F < 1$, $\ln \gamma_{<}$ has a shape that is independent of Q , A , and Θ ; $\ln \gamma_{<}$ scales with Q , compared with Q^2 for the truncated harmonic potential.

(iii) For $F > 1$, $\ln \gamma_{>}$ falls off exponentially in a frequency range that becomes narrower as Q increases.

E. Asymptotic behavior of the resonance curve

It is worth noting that the analytical expressions of Eqs. (5.25) and (5.27) are valid only for frequencies not too different from the plasma frequency. These expressions are not meant to predict the behavior of the resonance for $F \rightarrow 0$ or $F \rightarrow \infty$. Both of these limits can be treated exactly, however.

In the limit $F \rightarrow 0$ we can rewrite the Langevin equation as

$$\frac{\partial^2 x}{\partial \tau^2} + \frac{1}{Q} \frac{\partial x}{\partial \tau} + \frac{\partial}{\partial x} \left[\frac{x^2}{2} - \frac{1}{3\sqrt{6}} x^3 \right] = \xi(\tau) + A \cos \phi, \quad (5.29)$$

ϕ varies slowly with time, and we can take it as constant during the escape. We thus only need to calculate

$$\left\langle \exp \left[-\frac{\Delta U(\phi)}{k_B T} \right] \right\rangle_\phi$$

to obtain γ . The result in the limit of small A is

$$\ln \gamma = \frac{3}{2\Theta} \left[\frac{1}{\Theta} - \frac{1}{3} \right] A^2 \quad (F \ll 1), \quad (5.30)$$

which, apart from a numerical factor of order unity, is the same result as for the truncated harmonic oscillator at zero frequency. The enhancement does not vanish at very low frequencies but rather takes a small frequency-independent value, in contrast with Eq. (5.25). Taking Eq. (5.26) as an estimate of the $F=1$ value of $\ln \gamma$, we see that the ratio $\ln \gamma(F=1)/\ln \gamma(F=0)$ is of order of $4Q$. In the rest of the paper this $F=0$ value of $\ln \gamma$ is negligible except in the case $Q=5$.

In the limit $\Omega \rightarrow \infty$, the driving force induces a rapid oscillation of the coordinate x . The effect of the driving force is simply to renormalize the potential,⁵

$$U(x) \xrightarrow{F \rightarrow \infty} U(x) + \frac{1}{4} \frac{A^2}{F^4} \frac{d^2 U}{dx^2}. \quad (5.31)$$

This renormalization of the potential changes the barrier height. The enhancement is given by

$$\ln \gamma = \frac{A^2}{2\Theta F^4} \quad (F \gg 1), \quad (5.32)$$

which is qualitatively different from Eq. (5.15) in the limit $F \rightarrow \infty$. This expression shows that $\ln \gamma$ cannot decrease exponentially to zero as Eq. (5.27) would predict. One should not therefore take the exact analytical dependence of the sharp higher-frequency cutoff predicted by IM and LO too literally.

VI. NUMERICAL SIMULATIONS AND AN EMPIRICAL EXPRESSION FOR $\ln\gamma$

We have simulated the Langevin equation for a particle in a metastable well of the “washboard” potential, subjected to an external oscillating force. We used a discrete-time version of the equation in which the time step was $\frac{1}{100}$ of the oscillation period at the bottom of the well. We verified that this time step was sufficiently short to reproduce the dynamics of the system correctly by comparing the results with those obtained using significantly shorter time steps. Thermal noise was produced by a random-number generator based on a shift register. The number of steps during each run was 2.4×10^8 , corresponding to 2.4×10^6 oscillations. During this fixed length of time we recorded the number of escape events as a function of the frequency of the applied force. In addition to an increase in the number of steps, we improved our previous algorithm³ by following each escape event over the top of the barrier during each run instead of simply recording the population near the top of the well. Most of the simulations were carried out with $s = 0.73$ and $\Theta = \frac{1}{10}$, which were chosen to give reasonably low statistical errors without excessively long computer times. In the experiment the Θ parameter varied between $\frac{1}{14}$ and $\frac{1}{10}$.

As an initial check on our procedures we verified that the thermal-activation rate in the absence of any driving force ($A = 0$) was in agreement with theoretical predictions. In Fig. 14 we plot our simulated values of $\Gamma/\Gamma_{\text{TS}}$ vs Q ; here, $\Gamma_{\text{TS}} = (\omega_p/2\pi)\exp(-1/\Theta)$ is the prediction of the transition-state (TS) theory.⁴ Also shown are the predictions [Eq. (2.11)] of the theory of Büttiker *et al.*¹⁵ (BHL) for $\alpha = 1.4738$ in the limit of high Q , and Kramers’s result,⁴ which is valid in the limit of low Q . Given the present theoretical uncertainty in the intermediate ($Q \sim 1/\Theta$) regime, we feel that our numerical simulations are entirely adequate.

We turn next to the numerical simulation of resonant activation.

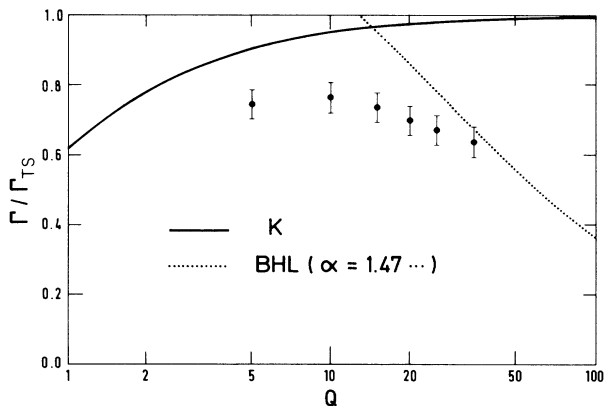


FIG. 14. Simulated values of $\Gamma/\Gamma_{\text{TS}}$ vs Q . Dotted line (BHL) is the prediction of Eq. (2.11) with $\alpha = 1.4738$. Solid line (K) is Kramers’s prediction for the moderate-damping case [Eq. (2.20b) in Hanggi’s review article, Ref. 4].

A. Resonant activation

In Fig. 15 we present numerical results for $\ln\gamma$ vs F for six values of Q ranging from 5 to 35. As Q was increased, A was reduced to keep the magnitude of the resonance approximately constant. As in our previously published preliminary data,³ the curves demonstrate the existence of a resonance in the enhancement response when the driving frequency is close to the plasma frequency. The resonance resembles the experimental data in that it is highly asymmetric: The low-frequency side is very broad with a shape that is almost independent of Q , while the high-frequency side becomes steeper as Q is increased. The curves always peak at a frequency less than the plasma frequency ($F < 1$) with a height that grows with both A and Q . To within the statistical error, all the curves have the same shape up to a dimensionless frequency roughly $1/Q$ below the peak. The only difference between these new results and our preliminary results is the somewhat more pronounced low-frequency tail which we believe results from an exact treatment of the dynamics of the particle during the escape.

To illustrate the dependence of the magnitude of the resonance on A , in Fig. 16 we plot $\ln\gamma$ vs A^2 for $F = 0.95$ and $Q = 10$. For small values of A we confirm that $\ln\gamma$ is proportional to A^2 , that is, to the power of the driving force. We refer to this behavior as the linear regime. As soon as $\ln\gamma$ is greater than about 1, however, it increases more slowly. For the remainder of this section we will focus on the linear regime.

We have also investigated the temperature dependence of $\ln\gamma$. In Fig. 17 we plot $(\ln\gamma)/A^2$ vs Θ^{-2} for simulations performed at $F = 0.92$ with $Q = 10$. A line corresponding to $\ln\gamma \propto \Theta^{-2}$ has been drawn through the data; within the statistical errors, the points lie on this line. Thus, our simulations confirm the IM-LO predictions that $\ln\gamma \propto A^2 Q / \Theta^2$ in the linear regime.

Finally, we compare the area under the resonance curve and the predictions of the sum rule. The results are shown in Table II. The sum rule is well obeyed in the mid- Q range, showing that the overall magnitude of the resonance effect is correctly reproduced in the numerical simulations. The discrepancy for the lower and higher values of Q could be explained by the statistical uncertainty in the baseline and by low-frequency contributions not taken into account by the range of integration.

The scatter in the simulated curves of Fig. 15 (which required a large amount of computer time) emphasizes the difficulty of performing a substantial number of simulations over a wide range of F to obtain a catalog of resonance shapes to which experimental data can be fitted. For this reason, we have found it desirable to construct an empirical expression for $\ln\gamma$ that can be tested against our simulations and then fitted to the experimental data to extract ω_p and Q simply and accurately.

B. Fit of the simulated enhancement response curves with an empirical function

Our empirical expression for $\ln\gamma$ has the following properties:

- (i) it retains the proportionality to $A^2 Q / \Theta^2$,

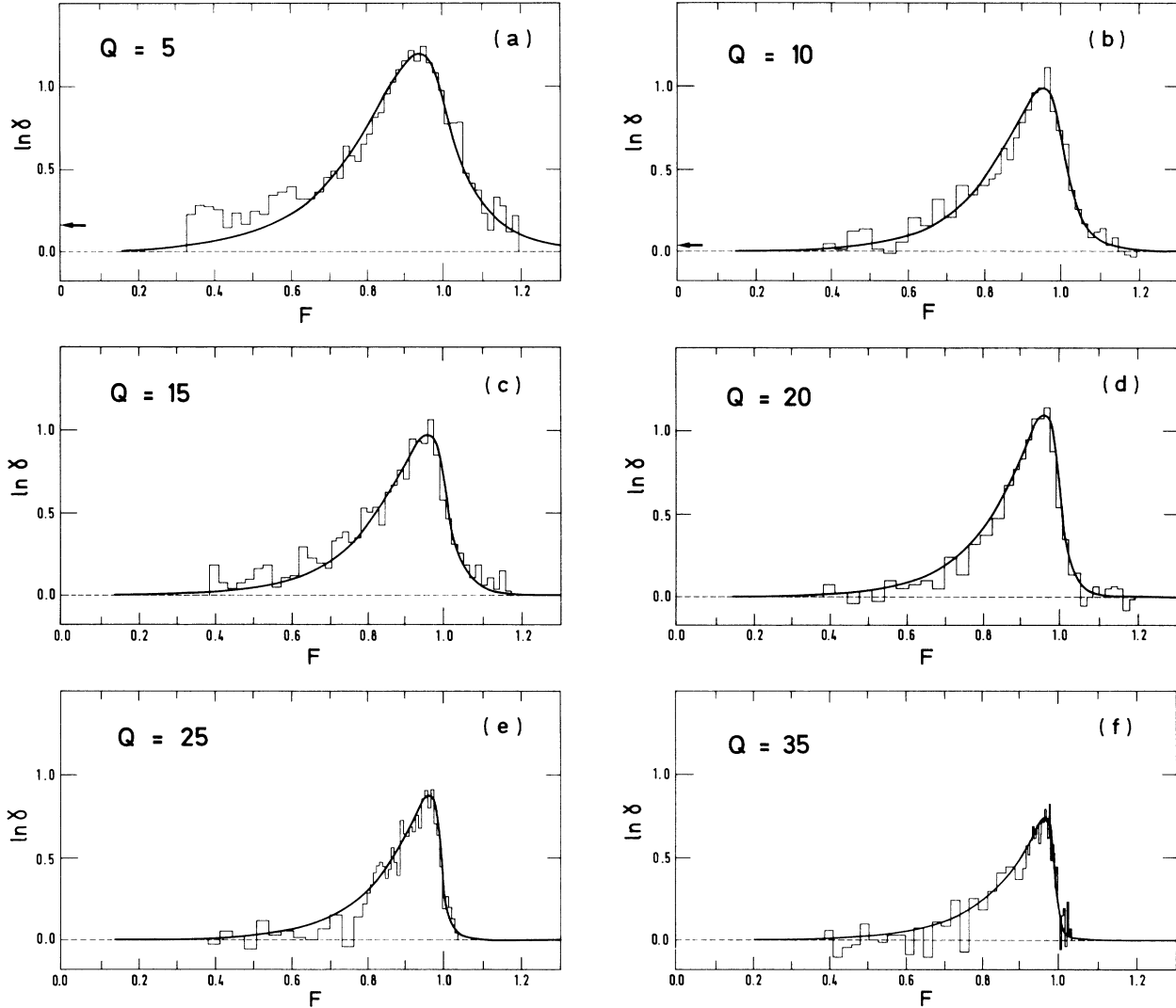


FIG. 15. Numerical simulations of $\ln \gamma$ vs $F = \Omega/\omega_p$ for six values of Q (stepped curves). Also shown are fits of the data by Eq. (6.1) (solid lines). The amplitude A of the driving force has been adjusted for each value of Q and is given in Table II.

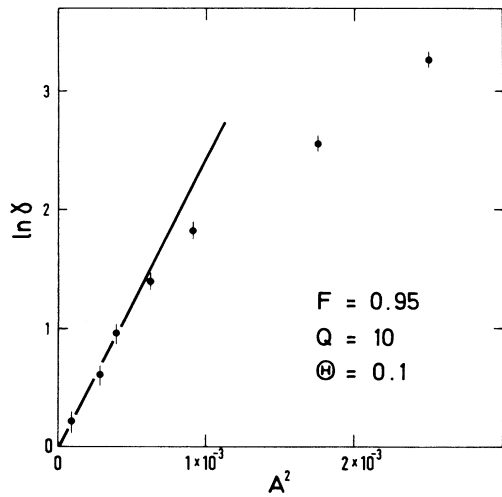


FIG. 16. Simulated values of $\ln \gamma$ vs A^2 . A straight line has been drawn through the three lowest data points to guide the eye.

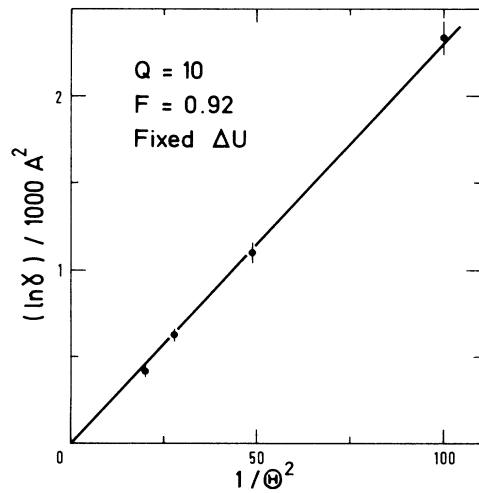


FIG. 17. Simulated values of $(\ln \gamma)/A^2$ vs Θ^{-2} for $Q=10$ and $F=0.92$. A line has been drawn through the data points to guide the eye.

TABLE II. Test of sum rule [Eq. (5.23)] with numerical simulation for six values of Q . F_{\min} and F_{\max} are the minimal and maximal dimensionless frequencies at which data are taken (see Fig. 15). Ideally, if $F_{\min}=0$ and $F_{\max}=\infty$, a value of 1 in the last column would mean that the data obeyed the sum rule exactly. In the simulations, $\Theta=\frac{1}{10}$.

Q	$A (\times 10^{-2})$	$\frac{4\Theta^2}{\pi Q A^2} \int_{F_{\min}}^{F_{\max}} \ln \gamma dF$
5	4.0	0.71
10	2.0	0.77
15	1.5	0.97
20	1.3	0.75
25	1.0	0.70
35	0.8	0.59

(ii) it retains the universality of the low-frequency shape, and

(iii) it contains a single shape parameter λ that depends only on Q .

The function is the convolution product of an exponential in $\lambda |F|$ with a function that describes the low-frequency behavior of the resonance (see Fig. 18),

$$\ln \gamma^{\text{fit}} = (c A^2 Q / \Theta^2) f(F), \quad (6.1)$$

where

$$f(F) = f_0(F) * [(\lambda/2) \exp(-\lambda |F|)]. \quad (6.2)$$

In Eq. (6.2), $*$ denotes a convolution product, and $f_0(F)$ is the following function:

$$f_0(F) = \begin{cases} e^{ux(1+vx)}, & x = F - 1 - d \leq 0 \\ 0, & x = F - 1 - d > 0. \end{cases} \quad (6.3)$$

The factor c is an overall scaling factor that would be a numerical constant if the sum rule were obeyed. The quantity d , where $|d| \ll 1$, allows us to slide the curve bodily along the frequency axis, if necessary. Equation (6.1) implies that the low-frequency wing will always have the same shape up to a frequency roughly $1/\lambda$ below the peak, while the high-frequency wing will cut off exponentially above the peak.

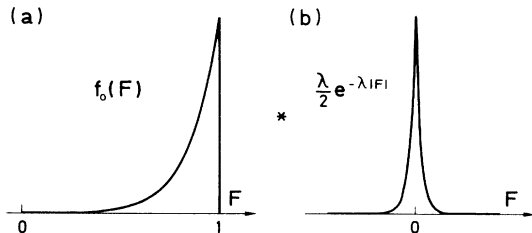


FIG. 18. The functions $f_0(x)$ and $(\lambda/2)\exp(-\lambda|x|)$ (with $\lambda=40$) that were convolved to fit the simulated resonant activation curves.

Carrying out the convolution, we find

$$f(F) = \frac{\lambda}{2} \left[\frac{e^{ux}}{\lambda+u} \left[1+vx - \frac{v}{\lambda+u} \right] + \frac{e^{\lambda x} - e^{ux}}{u-\lambda} \left[1 - \frac{v}{u-\lambda} \right] - \frac{vx e^{ux}}{u-\lambda} \right], \quad x \leq 0 \quad (6.4)$$

and

$$f(F) = \frac{\lambda}{2} e^{-\lambda x} \left[\frac{1}{u+\lambda} - \frac{v}{(u+\lambda)^2} \right], \quad x > 0. \quad (6.5)$$

By fitting $f(\lambda)$ to the numerical simulations below the peak, we chose $u=9$ and $v=-2$. To compare $f(\lambda)$ for $F \lesssim 1$ with the IM-LO theory, in Fig. 13 we have plotted it for $\lambda=\infty$ and 25. The curve for $\lambda=\infty$ agrees remarkably well with

$$(5\omega_p/36\Delta U) \frac{d\omega(E)}{dE} \Big|_F^{-1}$$

throughout the range, while that for $\lambda=25$ departs from it at a frequency roughly $1/\lambda=0.04$ below the peak, as we would expect.

We have fitted $\ln \gamma^{\text{fit}}$ to each of the simulated curves in Fig. 15 for the appropriate values of A , Q , and Θ using the values of λ and c plotted versus Q in Fig. 19. The

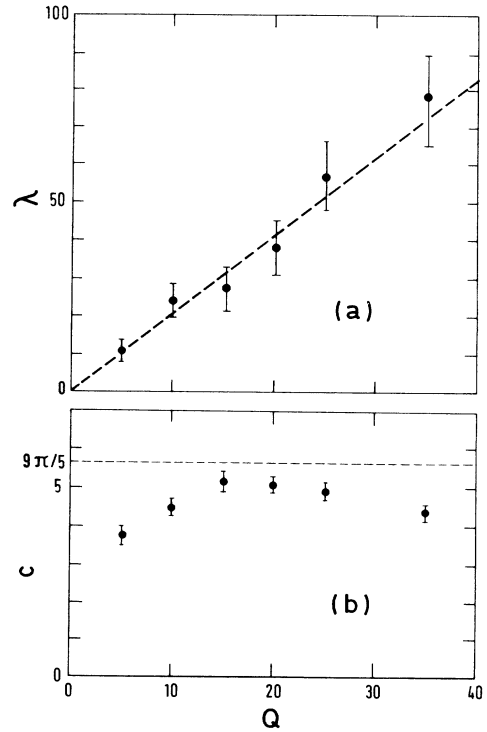


FIG. 19. Dependence of (a) λ and (b) c on Q extracted from the fits of $f(F)$ to the numerical simulations in Fig. 15. The dashed line in (a) is a least-squares fit of the data to a linear law $Q \propto \lambda$. The IM-LO value of $c=9\pi/5$ is shown for comparison in (b).

value of d was zero for the three lowest values of Q , 0.005 for $Q=20$, 0.01 for $Q=25$, and 0.02 for $Q=35$; the latter three values were chosen to improve the fit above the peak. In every case except $Q=5$ a good fit could be obtained. For $Q=5$ the simulated curve develops a very pronounced low-frequency tail incompatible with Eq. (6.3) but in agreement with Eq. (5.30). We see in Fig. 19 that, within the statistical uncertainty, λ scales with Q . The coefficient c varies slowly with Q for $Q > 10$, but drops markedly for $Q < 10$. We have indicated the value $9\pi/5$ corresponding to the asymptotic expression (5.25) for comparison. This behavior reflects the variation of the area under the resonance curve given in Table II. The statistical uncertainty shown by the error bars of Fig. 19 could be reduced by continuing the simulation for longer times.

C. Comparison of $\ln\gamma^{\text{fit}}$ with experiment

We are now in a position to use our empirical expression for $\ln\gamma$ to fit our experimental data. We scale the height of the curve arbitrarily (since A^2 is unknown experimentally), and adjust ω_p and λ until a best fit of the high-frequency side is obtained. The resulting curves are shown in Figs. 8 and 9, while the values of the fit parameters ω_p and λ are given in Table I, along with the corresponding estimates of Q , C , and R . It can be seen that the fit on the low-frequency side is poor, the shape of the discrepancy even varying from curve to curve.¹⁸ We believe that this discrepancy could come from the frequency-dependent loading of the junction by the mount which only crudely approaches an ideal infinitely long transmission line. A perturbation calculation carried out along the same lines as in Ref. 5 shows that $d\omega/dE$ is sensitive to frequency variations of C . The result of Fig. 9(b) (shunted junction), however, is remarkable. The high-frequency side is markedly less steep than for the unshunted junction and the value of $R = 8 \pm 2 \Omega$ deduced from λ (Table I) is in good agreement with the value of 10.7Ω measured from the I - V characteristic at $I \gg I_0$ of junction C . Given the discrepancy between the simulation and fit of Fig. 15(a), the low value of Q for this junction may explain why the low-frequency tail of the resonance is so important. In the case of the unshunted junctions A and B the resistance ($\sim 10^2 \Omega$) is also consistent with an estimated value of the admittance presented by the mount. Furthermore, there is good agreement between the fitted C and our *a priori* estimate of the junction capacitance. As we expect, C is relatively independent of the critical current. It is worth noting that although the resistive loading of the junction is dominated by losses in the mount, the reactive loading due to the mount is a small contribution to the total capacitance.

Finally, we compare various scaling properties of our data with predictions. Both the experimental data (Fig. 10) and simulations (Fig. 16) show that $\ln\gamma$ is linear in the square of the microwave amplitude for $\ln\gamma \lesssim 1$, rolling off at higher enhancements. In each of the experimental graphs, a point from the simulations has been plotted in the nonlinear regime. We see that the agreement between the experimental and simulated values of $\ln\gamma$ in the non-

linear regime is quite good. Equation (6.1) enables us to test the temperature dependence of resonant activation at fixed microwave frequency and amplitude. The enhancement factor $\ln\gamma$ is predicted to scale as A^2Q/Θ^2 , that is, $I_m^2 R \Delta U / \omega_p T^2$. In the experimental measurements leading to Fig. 11, ω_p and $\Delta U / k_B T$ were kept fixed; thus, we expect $\ln\gamma$ to scale as $1/T$. The inset of Fig. 11 shows that this scaling is well obeyed experimentally.

VII. CONCLUDING SUMMARY

We have presented measurements of the microwave-induced enhancement of the escape rate of a Josephson junction from its zero-voltage state. The measurements were made in the limit where the microwave amplitude is a weak perturbation on the thermal-noise amplitude. At a fixed power level, the enhancement is a resonant function of frequency. The resonance is asymmetric with a higher slope on the high-frequency side that becomes less steep when the junction is shunted with an external resistor, that is, when the damping is more important. We find that $\ln\gamma$ scales linearly with I_m^2 for $\ln\gamma \leq 1$ irrespective of the microwave frequency. Furthermore, $\ln\gamma$ scales with $1/T$ as we show by measuring γ as function of temperature for fixed values of the thermal escape rate and plasma frequency.

The above experimental features follow the theoretical predictions:

- (i) The shape of the resonance curve on the low-frequency side should be a universal function which depends only on the shape of the potential from which the particle escapes.
- (ii) On the high-frequency side the resonance curve rolls off exponentially with a characteristic frequency varying as $1/Q$.
- (iii) The height of the resonance curve should be of order $(9\pi/5)(\Delta U / k_B T) Q I_m^2 R / T \omega_p$.

Because the theory does not provide analytical predictions for the entire resonance curve, we have carried out numerical simulations of the curve for several values of Q . These simulations were used, in turn, to adjust the parameters of an empirical function that was constructed by interpolating the analytical theoretical predictions for the wings of the resonance curve. This empirical function is a simple convolution product of a universal function with a double exponential the width of which is proportional to Q^{-1} . This empirical function greatly facilitates the detailed comparison between the results from the simulations and the experiment.

We obtain good qualitative agreement between the observations and numerical simulations. However, the exact shape of the resonance curve on the low-frequency side is obtained only in one case for an unshunted junction. This discrepancy may be due to a frequency dependence of the damping factor Q arising from imperfections in the junction mount. Further experiments, with more careful microwave engineering of the mounts and the junctions are needed to confirm this point.

Two other puzzling features would also benefit from further investigations both theoretically and experimentally.

(i) We observe $\ln\gamma$ to be linear in the square of the amplitude for $\ln\gamma \lesssim 1$ at all frequencies, even well below and well above the position of the maximum of the response. Because of the sharp roll-off of the response above the peak frequency, this result implies that the range over which $\ln\gamma$ remains linear depends not simply on the amplitude of the driving force, but rather on the extent to which the average energy of the particle is increased by the driving force.

(ii) An interesting prediction of the theory is that the sharp high-frequency cutoff should be exponential. Far away from the plasma frequency, however, an exact calculation (Sec. V E) predicts a power-law dependence on frequency. Although both experiment and numerical simulations are well fitted by our empirical formula, which contains the exponential cutoff, it would be interesting to perform a more precise experiment to test the range of validity of this functional form.

We remark in passing that these two features seem to be specific to the classical regime ($\hbar\omega_p \ll k_B T$) and are not observed in the quantum regime ($\hbar\omega_p \gg k_B T$) when there are only a few quantized energy levels in the well.¹³ It would thus be a considerable advantage to have a theory valid for all frequencies and for powers outside the small power range. The generalization of the theory to take into account an arbitrary shunting admittance would enable one to use resonant activation to characterize this admittance experimentally.

Indeed, as we have seen, one important application of resonant activation is the determination of the parameter ω_p and Q and, hence, of C and R , for a Josephson junction. In this determination one, of course, has to assume that the admittance can be represented by a parallel combination of C and R in a wide range around the plasma frequency. We think this approximation is crude in our experiment due to imperfections of the junction mount. Nevertheless, the value measured for ω_p in this way is rather precise ($\pm 2\%$), while that for λ is much less precise ($\pm 20\%$). At present, the determination of Q from λ is even less accurate because of the statistical uncertainty arising from the simulations; extended calculations could, of course, reduce this uncertainty. For an unshunted junction our measurements show that the dissipation at frequencies $\sim \omega_p$ is dominated by losses in the leads. On the other hand, for our relatively-large-area junctions ($C \sim 10$ pF) the capacitance loading is relatively unimportant. We emphasize, however, that reactive loading is

likely to be substantial for smaller junctions ($C \lesssim 1$ pF). The application of this technique to determine the values of C and R required to interpret measurements of macroscopic quantum tunneling is presented in detail elsewhere.¹³

In concluding, we would like to reemphasize that the asymmetric shape of the enhancement response curve reflects the properties of the response of an anharmonic oscillator subjected to a sinusoidal perturbation. This response is fundamentally different from that of a harmonic oscillator to the same perturbation. As the particle escapes from the well, its oscillation frequency is continuously changing and it cannot be coherently pumped by the applied oscillating force, whatever its frequency. However, when the excitation frequency is below the oscillation frequency at the bottom of the well, there is an energy in the well at which the oscillation frequency matches the excitation frequency, making possible an energy transfer between the excitation force and the particle. The broad width of the resonance below the peak which is observed even for low damping is a direct consequence of the distribution of the oscillation frequencies in the well. The damping manifests itself not in the width of the resonance, but in the sharpness of the high-frequency cutoff of the response when the excitation frequency is scanned through the maximum oscillation frequency.

ACKNOWLEDGMENTS

We would like to thank Dr. R. Landauer for helpful discussions and Dr. P. Grigolini and Dr. T. Fonseca, Dr. B. I. Ivlev and Dr. V. I. Mel'nikov, Dr. A. I. Larkin and Dr. Yu. N. Ovchinnikov, and Dr. P. Hanggi for communicating their results prior to publication. One of us (J.M.M) gratefully acknowledges support from the National Science Foundation and IBM during the course of this research, while another (A.C.) thanks the University of California, Berkeley, for partial support. We gratefully acknowledge the use of the Microelectronics Facility in the Electronics Research Laboratory and the Electrical Engineering and Computer Science Department, University of California at Berkeley. This work was supported by the Commissariat à l'Énergie Atomique and the Director, Office of Energy Research, Office of Basic Energy Sciences, Materials Sciences Division of the U.S. Department of Energy, under Contract No. DE-AC0-76SF00098.

¹B. D. Josephson, *Phys. Lett.* **1**, 251 (1962).

²A. Barone and G. Paterno, *Physics and Applications of the Josephson Effect* (Wiley, New York, 1982).

³M. H. Devoret, J. M. Martinis, D. Esteve, and J. Clarke, *Phys. Rev. Lett.* **53**, 1260 (1984).

⁴H. A. Kramers, *Physica* **7**, 284 (1940). Also see the review by P. Hanggi, *J. Stat. Phys.* **42**, 105 (1986).

⁵L. D. Landau and E. M. Lifshitz, *Mechanics* (Pergamon, Oxford, 1960), pp. 80–93.

⁶See, for example, *Physics and Applications of the Josephson*

Effect, Ref. 2, Chap. 11.

⁷E. Ben-Jacob and D. J. Bergman, *Phys. Rev. A* **29**, 2021 (1984).

⁸T. Fonseca and P. Grigolini, *Phys. Rev. A* **33**, 122 (1986).

⁹B. I. Ivlev and V. I. Mel'nikov (unpublished).

¹⁰A. I. Larkin and Yu. N. Ovchinnikov, *J. Low Temp. Phys.* **63**, 317 (1986).

¹¹W. C. Stewart, *Appl. Phys. Lett.* **12**, 277 (1968); D. E. McCumber, *J. Appl. Phys.* **39**, 3133 (1968).

¹²T. A. Fulton and L. N. Dunkleberger, *Phys. Rev. B* **9**, 4760 (1974).

- ¹³J. M. Martinis, M. H. Devoret, and J. Clarke, *Phys. Rev. B* **35**, 4682 (1987).
- ¹⁴A. O. Caldeira and A. J. Leggett, *Ann. Phys. (N.Y.)* **149**, 374 (1983).
- ¹⁵M. Büttiker, E. P. Harris, and R. Landauer, *Phys. Rev. B* **28**, 1268 (1983).
- ¹⁶H. Risken and K. Voigtlaender, *J. Stat. Phys.* **41**, 825 (1985).

¹⁷The lower limit is from Ref. 10 and the upper from Ref. 9.

¹⁸In view of these variations and the improvement of the numerical simulations, we believe that the very good quantitative agreement between experimental results and simulations for the low-frequency tail of the resonance in Fig. 3 of Ref. 3 is only fortuitous.